



Cite this: DOI: 10.1039/c8nj02818d

Adsorptive denitrogenation of fuel over molecularly imprinted poly-2-(1*H*-imidazol-2-yl)-4-phenol microspheres†

 M. S. Abdul-quadir,^a R. van der Westhuizen,^b W. Welthagen,^b E. E. Ferg,^a
Z. R. Tshentu^a and A. S. Ogunlaja *^a

Molecularly imprinted poly-2-(1*H*-imidazol-2-yl)-4-phenol microspheres (MIPs) were prepared by suspension polymerization of 2-(1*H*-imidazol-2-yl)-4-vinylphenol in the presence of nitrogen containing compounds (N-compounds). Nitrogen containing compounds such as quinoline, pyrimidine and carbazole, largely found in fuel oils, were employed as templates in MIP synthesis. Isothermal titration calorimetric (ITC) studies revealed that quinoline/2-(1*H*-imidazol-2-yl)-4-phenol (PIMH) and pyrimidine/2-(1*H*-imidazol-2-yl)-4-phenol (PIMH) interactions were exothermic (-18.0 ± 4.8 and -28.1 ± 3.6 kJ mol⁻¹, respectively), while the carbazole/2-(1*H*-imidazol-2-yl)-4-phenol (PIMH) interaction was endothermic (3.3 ± 0.7 kJ mol⁻¹). Imprinted microspheres show selectivity for the various target nitrogen-containing compounds in fuel oil with adsorption capacities of 10.56 mg g⁻¹, 11.71 mg g⁻¹ and 10.84 mg g⁻¹ for pyrimidine, carbazole and quinoline, respectively. The removal of other stubborn nitrogen containing compounds from fuel oil demonstrates their potential application in the field of fuel denitrogenation.

Received 6th June 2018,
Accepted 30th June 2018

DOI: 10.1039/c8nj02818d

rsc.li/njc

1. Introduction

Fuel oil is one of the major sources of energy for industries and vehicles in many countries of the world, and it is obtained mainly from fossil sources. These fossil fuels contain many contaminants known as heteroatoms, *e.g.* nitrogen containing compounds, sulfur containing compounds and metals.^{1–3} The presence of nitrogen containing compounds such as basic nitrogen compounds (*e.g.* pyridine and its benzologues) and non-basic nitrogen compounds (*e.g.* pyrrole and its benzologues such as indoles and carbazoles) in fuel constitutes a major environmental and health concern even though their percentage in fuel is very small (less than 0.5%).^{4–9}

These organonitrogen compounds also give rise to fuel instability during storage due to the formation of gums, colours and sediments. Second, compounds such as quinoline and related molecules are capable of binding strongly on catalyst surfaces, hence, deactivating refining catalyst.^{10–15} The most harmful effect of nitrogen molecules in fuel is the emission of NO_x into the environment which is a major source of pollution

that causes many environmental hazards like acid rain and photochemical smog. The pollution effect of this NO_x also includes formation of small particles which penetrate the lungs and cause respiratory diseases such as bronchitis and asthma. Due to the harm posed by these gases, the US EPA aimed at improving air quality mandated the reduction of nitrogen content in diesel fuel to ultra-low levels of <1 mg L⁻¹.^{16,17}

Several methods have been reported on the denitrogenation of fuel and these include catalytic hydrodenitrogenation (HDN),³ which takes place under extreme temperature and pressure,^{18–20} and it is known to be kinetically slow.⁴ HDN is effective in the removal of the less bulky non-refractory nitrogen containing compounds. The technique is ineffective in the elimination of refractory organonitrogen compounds such as highly alkylated carbazole and quinoline,²¹ thus, leading to a fall out in the mandated nitrogen specification of <1 mg L⁻¹. Extractive denitrogenation is another method that has been applied for the elimination of nitrogen containing compounds (NCCs) in fuel.²² This method suffers from the fact that other compounds can also be extracted along with NCCs. Adsorptive denitrogenation (ADN) is the most recent method that is being applied to remove NCCs from fuel oil. So far, many adsorbents such as activated carbon, zeolites, silica, and ion-exchange resins have been used in ADN.^{23–26} Nevertheless, most of the adsorbents suffer from limitations such as that they may complex with other compounds in the fuel. Recently, porous materials, including mesoporous materials like metal organic frameworks (MOFs),

^a Department of Chemistry, Nelson Mandela University, P.O. Box 77000, Port Elizabeth 6031, South Africa. E-mail: adeniyi.ogunlaja@mandela.ac.za; Tel: +27 46 504 3061

^b Analytical Technology, Sasol Technology (Pty) Limited, P.O. Box 1, Sasolburg 1947, South Africa

† Electronic supplementary information (ESI) available. See DOI: 10.1039/c8nj02818d

have been used in the denitrogenation of fuel (offering adsorption capacities of above 150 mg g^{-1}).¹ Ahmed *et al.* (2014) also demonstrated that an adsorption capacity of 357 mg g^{-1} for quinoline using MIL-100(Fe) can be achieved at an equilibrium time of 120 min and an adsorption capacity of 417 mg g^{-1} can be achieved when $\text{AlCl}_3(2.5\%)/\text{MIL-100(Fe)}$ was employed.²⁷ A 17% improvement in the adsorption of quinoline was attributed to the Lewis acid–base interaction between AlCl_3 and quinoline.²⁷ These MOFs displayed fast adsorption kinetics/rates, with high adsorption capacities; nevertheless, MOFs are not equally selective to NCCs.^{28–33} Hence, there is a need to develop more selective sorbents that can remove the NCCs from fuel.³⁴ Cao *et al.* (2014) recently developed indole-MIPs which gave an adsorption capacity of 31.80 mg g^{-1} at an equilibrium time of 90 min. It was further reported that the synthesised indole-MIPs also selectively removed stubborn non-nitrogen indole compounds from the fuel oil.³⁵ Yang *et al.* (2013) designed $\text{SiO}_2@\text{MIPs}$ for the selective removal of indole and carbazole type compounds. In their study, an adsorption capacity of 60 mg g^{-1} was attained in 150 min and a corresponding adsorption amount of 23.54 mg g^{-1} was attained in simulated oil (100 mg L^{-1}).³⁶

To the best of our knowledge, imprinted 1*H*-imidazol-2-yl-4-phenol based microspheres have not been prepared as denitrogenation adsorbents. Hence, for the first time in this study, we describe the selective adsorption of nitrogen containing compounds (such as quinoline, carbazole and pyrimidine) over molecularly imprinted poly-2-(1*H*-imidazol-2-yl)-4-phenol microspheres. The formation of intense green coloured pyrimidine imprinted poly-2-(1*H*-imidazol-2-yl)-4-phenol microspheres was also observed for the first time and characterised spectroscopically for its absorption band. A combined experimental and spectroscopic study was adopted to gain a fundamental understanding of the possible interactions responsible for adsorption.

2. Experimental

2.1 Materials

4-Bromo-2-hydroxybenzaldehyde, glyoxal trimer dihydrate, ethylene glycol dimethacrylate, quinoline, carbazole and pyrimidine were purchased from Sigma Aldrich, South Africa.

2.2 Instrumentation

FT-IR spectra ($4000\text{--}400 \text{ cm}^{-1}$) were run on a Bruker, Tensor 27 platinum ATR-FTIR spectrometer. The ^1H NMR spectra of ligands and monomer were recorded on a Bruker 400 MHz spectrometer in $\text{DMSO-}d_6$. Thermogravimetric analyses of imprinted and non-imprinted microspheres were performed using a Perkin-Elmer TGA 7 thermogravimetric analyser (TGA). Typically, the samples were heated at a rate of $10 \text{ }^\circ\text{C min}^{-1}$ under a constant stream of nitrogen gas. Microspheres were imaged using a TESCAN Vega TS 5136LM scanning electron microscope (SEM). Before images were taken, the microspheres were coated to prevent surface charging and to protect the surface material from thermal damage by the electron beam. Nitrogen adsorption/desorption isotherms were measured at

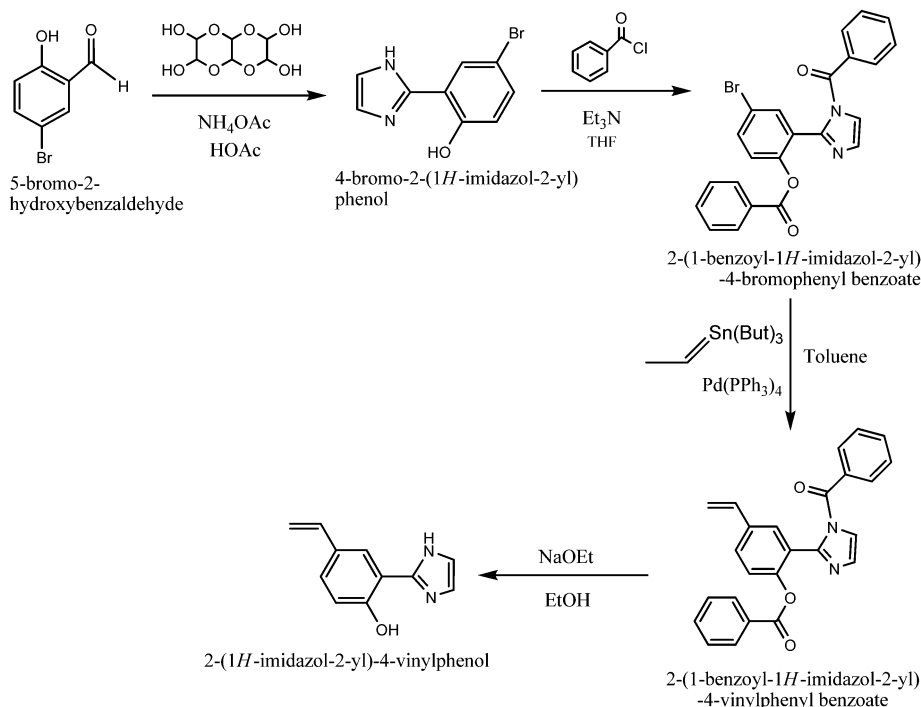
77 K using a TriStar II 3020 3.02, Surface Area and Porosity Analyzer by Micromeritics Instrument Corporation. Prior to each measurement, microspheres were degassed at $90 \text{ }^\circ\text{C}$ for 24 h. The BET surface area, total pore volume and pore size distribution were calculated from these isotherms. The solid reflectance spectra of the metal complexes were recorded on a Shimadzu UV-VIS-NIR Spectrophotometer UV-3100 with a MPCF-3100 sample compartment with samples mounted between two quartz discs which fit into a sample holder coated with barium sulfate. The spectra were recorded over the wavelength range of 2000–250 nm, and the scans were conducted at a medium speed using a 20 nm slit width. LECO Pegasus GC \times GC-HRT was employed to monitor the adsorption of organonitrogen compounds in diesel. Injection: split injection (100:1) at $250 \text{ }^\circ\text{C}$; primary column: Stabilwax (Restek), $30 \text{ m} \times 250 \text{ } \mu\text{m}$ ($0.25 \text{ } \mu\text{m}$); secondary column: Rxi-5 (Restek), $1.5 \text{ m} \times 100 \text{ } \mu\text{m}$ ($0.1 \text{ } \mu\text{m}$); carrier gas: helium, at a constant flow rate of 1.2 mL per minute; primary oven program: $40 \text{ }^\circ\text{C}$ (0.1 minute) to $260 \text{ }^\circ\text{C}$ (78.4 min) at $3 \text{ }^\circ\text{C per minute}$; secondary oven program: $45 \text{ }^\circ\text{C}$ (0.1 minute) to $265 \text{ }^\circ\text{C}$ (56 minute) at $3 \text{ }^\circ\text{C per minute}$; modulator offset: $15 \text{ }^\circ\text{C}$; modulation frequency: 8 seconds; hot time: 2 seconds; MS: LECO Pegasus 4D GC \times GC-TOFMS; ionization: electron ionization at 70 eV; source temperature: $250 \text{ }^\circ\text{C}$; stored mass range: 30 to 500 u; acquisition rate: 100 spectra per second.

2.3 Synthesis of imprinted microspheres

Prior to the synthesis of imprinted microspheres, the monomer 2-(1*H*-imidazol-2-yl)-4-vinyl phenol was synthesized by a method reported by Sellergren and co-workers,³⁷ with a few modifications.

2.3.1 Synthesis of the precursor 4-bromo-2-(1*H*-imidazol-2-yl) phenol. 4-Bromo-2-hydroxybenzaldehyde (10 g, 0.05 mol) and glyoxal trimer dehydrate (10.5 g, 0.05 mol) were added into 200 mL of glacial acetic acid and brought to reflux under nitrogen until they dissolved and then ammonium acetate (36 g, 0.05 mol) was added followed by continuous reflux for 4 h. After cooling to room temperature, the solution was poured into 2 L of water and filtered on celite. The dark brown filtrate was made basic by the addition of aqueous ammonia and the yellow precipitate formed was filtered and dried. The product was dissolved in acetone and refluxed with activated carbon for an hour. This was filtered on celite and concentrated on a rotavapor to give a purple product weighing 1.5 g. This was further purified on a silica column with ethyl acetate and ethanol as eluents (ratio 1:1). This was then concentrated using a rotavap and the solid product was weighed (Scheme 1). Yield = 22%. Melting point = $240\text{--}242 \text{ }^\circ\text{C}$. FT-IR (cm^{-1} , neat): 3368, 2414, 1586, 1530, 1494, 1463, 1280, 1252. ^1H NMR (400 MHz, $\text{DMSO-}d_6$): 12.44 (s, 1H), 8.09 (d, 1H), 7.38 (d, 2H), 7.07 (br-s, 2H), 6.92–6.90 (d, 1H). ^{13}C NMR (400 MHz, $\text{DMSO-}d_6$): 159.86, 155.49, 131.98, 126.62, 123.98, 119.90, 115.34, 110.62. Anal. calcd (found) for $\text{C}_9\text{H}_7\text{BrN}_2\text{O}$ (%): C, 45.22 (44.95); H, 2.95 (3.203); N, 11.72 (10.71).

2.3.2 Synthesis of 2-(1-benzoyl-1*H*-imidazol-2-yl)-4-bromophenyl benzoate. 4-Bromo-2-(1*H*-imidazol-2-yl) phenol (0.8 g, 0.003 mol) was dissolved in 30 mL of THF and triethylamine (0.61 g, 0.006 mol) was added followed by benzoyl chloride



Scheme 1 The synthesis scheme for 2-(1H-imidazol-2-yl)-4-vinyl phenol.

(0.84 g, 0.006 mol). The solution was stirred overnight and then filtered. The filtrate was concentrated to give a purple solid which was digested in diethyl ether and washed in the same solvent. A yield of 40% was observed (Scheme 1). Yield = 15.13%. Melting point = 131–133 °C. FT-IR (cm^{-1} neat): 1738, 1664, 1600, 1577, 1474, 1444, 1396, 1260. ^1H NMR (400 MHz, DMSO-d_6): 7.83 (m, 2H), 7.74 (M, 1H), 7.52 (m, 5H), 7.56 (m s., 1H), 7.42 (M, 4H). ^{13}C NMR (400 MHz, DMSO-d_6): 166.64, 163.57, 147.12, 134.11, 134.03, 133.07, 133.37, 130.75, 134.11, 130.34, 129.58, 129.17, 128.51, 127.88, 125.04, 121.97, 118.01. Anal. calcd (found) for $\text{C}_{23}\text{H}_{15}\text{BrN}_2\text{O}_3$ (%): C, 61.76 (60.08); H, 3.38 (3.55); N, 6.26 (6.42).

2.3.3 Synthesis of 2-(1-benzoyl-1H-imidazol-2-yl)-4-vinylphenyl benzoate. 2-(1-Benzoyl-1H-imidazol-2-yl)-4-bromophenyl benzoate (1 g, 2.24 mol) was dissolved in warm toluene. Palladium tetrakis(triphenylphosphine) (0.052 g, 0.045 mol) was added followed by the addition of tributyl (vinyl) tin (0.65 mL, 2.24 mol) and a trace of 3,5-diterbutylcatechol. The mixture was heated to reflux under nitrogen for 5 h. After cooling, it was filtered and the filtrate was concentrated to give a yellow sticky liquid. This was dissolved in 40 mL of acetonitrile and 20 mL of hexane was added for washing the resulting solution. The lower layer of the two immiscible liquids was run into a beaker; it is yellow and contained the product. This was concentrated and gave a yellow solid to which diethyl ether was added which coagulated it into a solid which was filtered. Yield: 85% (Scheme 1). Melting point = 122–124 °C. FT-IR (cm^{-1} neat): 1737, 1710, 1600, 1500, 1450, 1259. ^1H NMR (400 MHz, DMSO-d_6): 7.83 (m, 2H), 7.76 (s, 1H), 7.61–7.48 (m, 5H), 7.34–7.22 (m, 5H), 7.20 (M, 2H), 6.80 (m, 1H vinyl-H), 5.90 (d, 1H vinyl-H), 5.36 (d, 1H vinyl-H); ^{13}C NMR (400 MHz, DMSO-d_6): 166.78, 163.79, 147.26, 144.08,

133.94, 130.87, 129.54, 128.78, 128.46, 122.95, 121.65, 115.28. Anal. calcd (found) (%) for $\text{C}_{25}\text{H}_{18}\text{N}_2\text{O}_3$: C, 76.13 (76.05); H, 4.60 (4.84); N, 7.10 (6.28).

2.3.4 Synthesis of 2-(1H-imidazol-2-yl)-4-vinylphenol. 0.45 g of 2-(1-benzoyl-1H-imidazol-2-yl)-4-vinylphenyl benzoate was dissolved in 10 mL of ethanol. Sodium ethoxide was prepared separately by adding 50 mg of sodium in dry ethanol (50 mg). This was then added to the product solution drop wise till the mixture becomes yellow when it was concentrated and dissolved in 50 mL of 0.20 mol NaOH. The pH was adjusted to 10 by adding 0.1 mol HCl until the solution becomes cloudy; the precipitate was filtered and centrifuged and then washed with ice cold methanol followed by cold diethyl ether to give a pure cream solid (Scheme 1). Yield: 37.7%. Melting point = 133–134 °C. FT-IR (cm^{-1} , neat): 3369, 2918, 1609, 1532, 1494, 1464, 1413, 1279, 1253. ^1H NMR (400 MHz, DMSO-d_6): 14.28 (s, 1H), 8.05 (s, 1H), 7.33 (d, 1H), 6.90 (d, 1H), 6.70–6.62 (m, 1H vinyl-H), 5.90–5.86 (d, 1H vinyl-H), 5.23–5.20 (d, 1H vinyl-H). ^{13}C NMR (400 MHz, DMSO-d_6): 155.50, 144.86, 131.98, 127.81, 126.63, 118.97, 115.35, 109.87. Anal. calcd (found) for $\text{C}_{11}\text{H}_{10}\text{N}_2\text{O}$ (%): C, 70.97 (71.00); H, 5.40 (5.41); N, 15.02 (15.01). ^1H -NMR spectra of (A) 4-bromo-2-(1H-imidazol-2-yl) phenol, (B) 2-(1-benzoyl-1H-imidazol-2-yl)-4-bromophenyl benzoate, (C) 2-(1-benzoyl-1H-imidazol-2-yl)-4-vinylphenyl benzoate and (D) 2-(1H-imidazol-2-yl)-4-vinyl phenol are all presented in Fig. S1, ESI.†

2.3.5 Synthesis of imprinted poly-2-(1H-imidazol-2-yl)-4-phenol microspheres. 2-(1H-Imidazol-2-yl)-4-vinylphenol (1.86 g) was dissolved in a solution containing 2 mL of ethylene glycol dimethacrylate and 1 mL of toluene in the presence of nitrogen containing compound(s) (carbazole (0.176 g, 0.001 mol), quinoline (0.118 mL, 0.001 mol) and pyrimidine (0.08 g, 0.001 mol)

were added separately to the organic phase) (Scheme 2). After homogeneity was achieved, 0.02 g of benzoyl peroxide was added to the organic mixture. The resulting organic solution was transferred in drops into a 100 mL solution containing polyvinyl alcohol (PVA) (0.025 g) and NaCl (0.07 g) at 80 °C and under stirring at 400 rpm. The reaction was allowed to proceed for 7 h under an argon atmosphere, after which the resulting microspheres were collected by filtration.

Imprinted template molecules (nitrogen containing compounds) were removed by washing the microspheres *via* soxhlet extraction with a solution mixture of warm-to-hot methanol and acetonitrile (1 : 1) until no templates was detected on the GC-FID. The synthetic routes for the formation of nitrogen-imprinted microspheres are similar to the steps described for the non-imprinted microspheres (Section A of ESI†).

2.4 Adsorption and desorption studies of model nitrogen compounds

2.4.1 Adsorption studies of model nitrogen compounds.

Adsorption studies of nitrogen compounds were performed by (i) batch process for better understanding of the adsorption kinetics, selectivity and isotherms, and (ii) solid phase extraction (SPE) process in the reusability studies. To perform the batch adsorption studies, imprinted polymer microspheres (50 mg) was weighed into screw-capped vials containing 3 mL

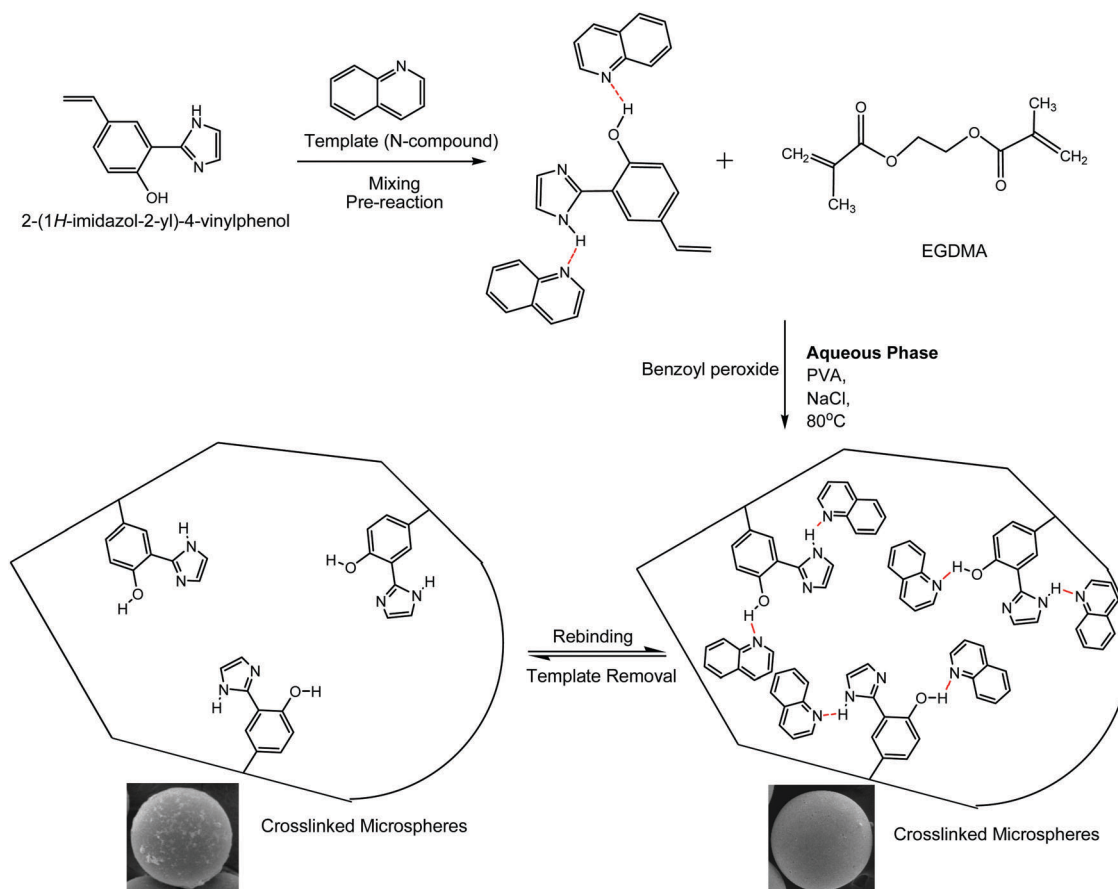
of nitrogen compounds (120 mg L^{-1}) alongside other molecules. The screw-capped vials containing nitrogen compounds were subjected to mechanical agitation at 100 rpm for 12 h. The progress of adsorption of the various nitrogen compounds was followed by withdrawing aliquots for measurement after every hour. Adsorption capacity, q_e (mg g^{-1}), was calculated from eqn (1).

$$q_e = \frac{V(C_0 - C_e)}{W} \quad (1)$$

where C_0 is the initial concentration (mg L^{-1}), C_e the equilibrium concentration (mg L^{-1}), W the weight of microspheres (g) and V the volume (L). Molecularly imprinted microspheres employed for adsorption were regenerated for re-usability by washing microspheres with a warm solvent mixture of acetonitrile and methanol (1 : 1). The adsorption kinetics and isotherm protocols are presented in the ESI.†

2.4.2 Adsorption selectivity studies of imprinted microspheres.

Selectivity studies were carried out to evaluate the loading capacity and selectivity of molecularly imprinted poly-2-(1*H*-imidazol-2-yl)-4-phenol microspheres. 50 mg of imprinted microspheres were added to vials and mixed with a 3 mL solution mixture of nitrogen containing compounds (quinoline, carbazole and pyrimidine), dibenzothiophene and naphthalene (120 mg L^{-1} each); the adsorption equilibrium was reached after 12 h. In order to quantitatively estimate the adsorption selectivity of various adsorbents for



Scheme 2 Scheme for the synthesis of quinoline imprinted poly-2-(1*H*-imidazol-2-yl)-4-phenol microspheres.

each compound a selectivity factor was used, which is expressed as follows:

$$\alpha_{i-r} = (q_i/q_r) - (C_{e,i}/C_{e,r})$$

where q_i and q_r are the adsorption capacities (mg g^{-1}) of compound i and the reference compound r at equilibrium, respectively. $C_{e,i}$ and $C_{e,r}$ (mg L^{-1}) are the equilibrium concentrations of compound i and the reference compound r , respectively. Naphthalene was selected as a reference compound in this study.

2.5 Thermodynamic studies

2.5.1 Isothermal titration calorimetry (ITC) and Van't Hoff experiments. ITC was employed for the determination of the degree of molecule–molecule interactions in solution.^{38–47} For this experiment, N-compounds–PIMH titration was performed on a modular titration nanocalorimeter with an injection volume of $10 \mu\text{L}$, a time spacing of 10 min between injections and a stirring speed of 40 rpm and at $25 \text{ }^\circ\text{C}$. The reference cell was left empty.

Van't Hoff experiments for all model organonitrogen compounds were carried out at 30, 35, 40 and $45 \text{ }^\circ\text{C}$ by using a batch adsorption process. Aliquots of analyte solutions were withdrawn at every 20 min intervals and analysed by using a GC-FID.

3. Results and discussion

3.1 FT-IR and UV-Vis spectroscopy

FT-IR analyses of imprinted and non-imprinted microspheres are as follows: non-imprinted microspheres: FT-IR (cm^{-1}): $3371 \nu(\text{O-H})$, $1726 \nu(\text{C=O})$, $1630 \nu(>\text{NH})$, $1289 \nu(\text{C-N})$, $1148 \nu(\text{C-O-C})$. Carbazole-imprinted microspheres: FT-IR (cm^{-1}): $3393 \nu(\text{O-H})$, $1722 \nu(\text{C=O})$, $1650 \nu(>\text{NH})$, $1233 \nu(\text{C-N})$, $1111 \nu(\text{C-O-C})$; pyrimidine-imprinted microspheres: FT-IR (cm^{-1}): $3563 \nu(\text{O-H})$, $1720 \nu(\text{C=O})$, $1650 \nu(>\text{NH})$, $1231 \nu(\text{C-N})$, $1140 \nu(\text{C-O-C})$; quinoline-imprinted microspheres: FT-IR (cm^{-1}): $3408 \nu(\text{O-H})$, $1721 \nu(\text{C=O})$, $1630 \nu(>\text{NH})$, $1260 \nu(\text{C-N})$, $1156 \nu(\text{C-O-C})$. FT-IR spectra of (i) non-imprinted microspheres, (ii) carbazole-imprinted microspheres, (iii) pyrimidine-imprinted microspheres and (iv) quinoline imprinted microspheres are all presented in Fig. S2 of ESI.† The diffuse reflectance spectra of non-imprinted microspheres, quinoline-imprinted microspheres (QUNMIPs), and carbazole-imprinted microspheres (CARMIPs) exhibited a similar absorption pattern, except for pyrimidine-imprinted microspheres (PYMMIPs) (Fig. 1). The UV spectra of the various polymer microspheres show one sharp absorption maximum at around 346–356 nm which is mostly assigned to $n \rightarrow \pi^*$ transition. Transitions ($n \rightarrow \pi^*$) for non-imprinted microspheres, pyrimidine-imprinted microspheres (PYMMIPs), quinoline-imprinted microspheres (QUNMIPs) and carbazole-imprinted microspheres (CARMIPs) are observed at 354 nm, 346 nm, 353 nm and 356 nm, respectively. Pyrimidine-imprinted microspheres (PYMMIPs) also displayed another band appearing at 733 nm (Fig. 1), thus confirming the interaction between 2-(1*H*-imidazol-2-yl)-4-phenol and PYM in crosslinked microspheres resulting in a possible intermolecular transition, and

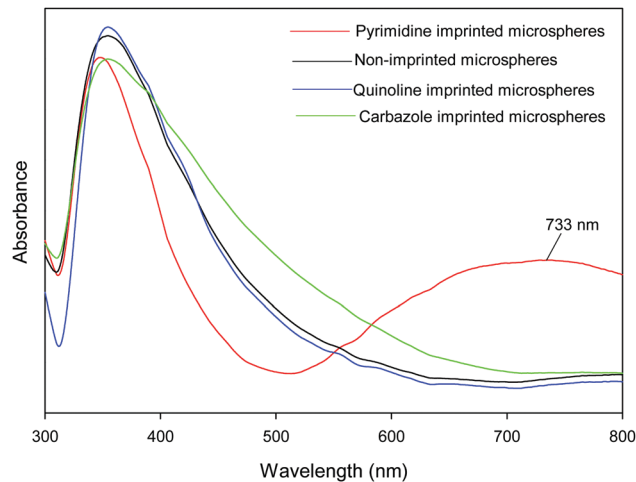


Fig. 1 Diffuse reflectance electronic spectra of non-imprinted microspheres, pyrimidine-imprinted microspheres (PYMMIPs), quinoline-imprinted microspheres (QUNMIPs) and carbazole-imprinted microspheres (CARMIPs).

hence PYMMIPs appear with a light blue-green colour.⁴⁸ Images of the various microspheres are provided in Fig. S3 in ESI.†

3.2 Thermogravimetric analysis (TGA) of non-imprinted and imprinted microspheres

Polymer microspheres (imprinted and non-imprinted) displayed distinct weight losses at ranges of around $90\text{--}140 \text{ }^\circ\text{C}$, $250\text{--}360 \text{ }^\circ\text{C}$ and $400\text{--}600 \text{ }^\circ\text{C}$ under a nitrogen atmosphere.

3.2.1 Non-imprinted microspheres (NIPs). NIPs presented a decomposition pattern with three distinct weight losses at around $280 \text{ }^\circ\text{C}$, $450 \text{ }^\circ\text{C}$ and $500 \text{ }^\circ\text{C}$ (Fig. 2). An observed 4% weight loss around $310 \text{ }^\circ\text{C}$ was assigned to loosely bound organic molecules within the microspheres. The decomposition of non-imprinted microspheres' backbone began to occur only at temperatures of around $320 \text{ }^\circ\text{C}$ to about $450 \text{ }^\circ\text{C}$, hence resulting in a total polymer weight loss of 68%. A further microsphere collapse (about 12%) occurred between 500 and $600 \text{ }^\circ\text{C}$.

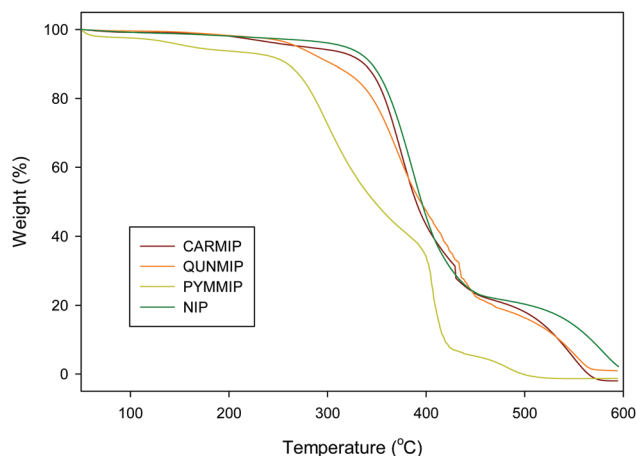


Fig. 2 TGA profile of carbazole-imprinted microspheres (CARMIPs), quinoline-imprinted microspheres (PYMMIPs), pyrimidine-imprinted microspheres (PYMMIPs) and non-imprinted microspheres under a nitrogen atmosphere.

3.2.2 Quinoline-imprinted microspheres (QUNMIPs). The quinoline-imprinted microspheres gave similar decomposition patterns as NIPs (280 °C, 450 °C and 500 °C). 5% weight loss attributed to strongly held (intramolecular) solvent molecules within the microspheres was observed at around 280 °C, followed by a rapid decomposition of the quinoline-imprinted polymer backbone occurring from 300 °C to a temperature of about 450 °C (Fig. 2). A total weight loss of 70% was reported. A further collapse, >10%, was reported to occur between 500 and 570 °C.

3.2.3 Pyrimidine-imprinted microspheres (PYMMIPs). The pyrimidine-imprinted microspheres (PYMMIPs) presented three distinct weight losses at around 250–320 °C, 400 °C and 470–500 °C. Pyrimidine-imprinted microspheres displayed a 9% weight loss at 250 °C and this is attributed to bonded solvent molecules. A further two-step polymer backbone decomposition was observed in the range of 280–400 °C (weight loss, 51%) and 400–420 °C (weight loss, 20%). The final decomposition (weight loss, 8%) occurred between 420 and 520 °C (Fig. 2).

3.2.4 Carbazole-imprinted microspheres (CARMIPs). The carbazole-imprinted microspheres (CARMIPs) presented two distinct weight losses at around 320 °C and 450 °C. A gradual 10% weight loss attributed to bonded (or intramolecular) solvents was observed at a temperature of up to 320 °C, followed by a rapid one-step polymer backbone disintegration in the temperature range of 320–450 °C (weight loss, 68%). The final decomposition (weight loss, 20%) was noticed at temperatures between 450 and 580 °C (Fig. 2).

The observed thermograms (Fig. 2) indicated that non-imprinted microspheres displayed a compact structure with high thermal stability. By contrast, imprinted microspheres have a loose structure due to the presence of pores (cavities created) within the material, and this was evident from the observed degradation patterns. Generally, porogen (solvent for polymerization) on the template influences the morphology, temperature stability and swelling capacity of the resultant polymers.^{49,50}

3.3 Scanning electron microscopy (SEM) and energy dispersive spectroscopy (EDS) of non-imprinted and imprinted microspheres

The SEM micrographs of non-imprinted and imprinted microspheres are presented in Fig. 3. Varying diameter ranges were observed with all microspheres, non-imprinted microspheres (290–367 μm), quinoline-imprinted microspheres (106–204 μm), pyrimidine-imprinted microspheres (210–255 μm) and carbazole-imprinted microspheres (173–280 μm). The images revealed the loose structure of the imprinted microspheres and the presence of numerous cavities and roughness on the microsphere surface. By contrast, the structure of non-imprinted microspheres was more compact and presented a smooth surface (Fig. 3). SEM images confirmed that some of the quinoline and pyrimidine imprinted polymers are irregular in shape (Fig. 3), while carbazole imprinted microspheres displayed more pores on their surface. The observed difference in polymer microsphere size and morphology was probably due to the different template molecules employed in the polymerization step.⁵¹

EDS images of the various non-imprinted and imprinted microspheres are presented in Fig. S4 (ESI[†]). Chemical characterization

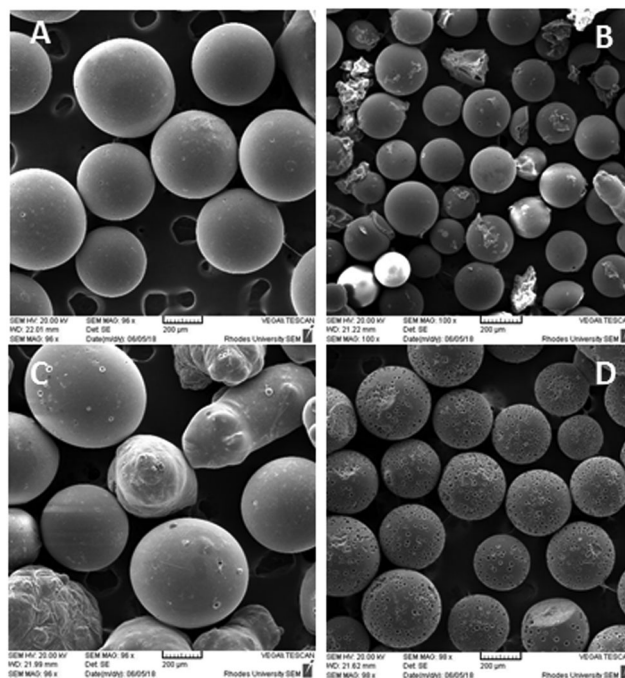


Fig. 3 Scanning electron micrograph (SEM) images of (A) non-imprinted microspheres, (B) quinoline-imprinted microspheres (QUNMIPs), (C) pyrimidine-imprinted microspheres (PYMMIPs) and (D) carbazole-imprinted microspheres (CARMIPs).

of microspheres after template removal was explored. The EDS study confirmed that the chemical integrity of the microspheres was preserved even after washing the templates off the microspheres.

3.4 BET surface area

Barrett–Emmett–Teller (BET) and Barrett–Joyner–Halenda (BJH) models was employed for the calculation of the surface area and the average pore size of (A) non-imprinted microspheres, (B) quinoline-imprinted microspheres (QUNMIPs), (C) pyrimidine-imprinted microspheres (PYMMIPs) and (D) carbazole-imprinted microspheres (CARMIPs). The nitrogen adsorption–desorption isotherms of non-imprinted microspheres and imprinted microspheres are shown in Fig. S5 (ESI[†]). Specific pore sizes and surface areas of non-imprinted microspheres and imprinted microspheres are shown in Table 1. The cavities created in non-imprinted microspheres, pyrimidine-imprinted microspheres (PYMMIPs), quinoline-imprinted microspheres (QUNMIPs), and carbazole-imprinted microspheres (CARMIPs) showed well defined pore openings with pore diameters of 27.1 ± 5.4 Å or 2.7 ± 0.5 nm; 51.6 ± 7.9 Å or 5.2 ± 0.8 nm; 60.9 ± 4.1 Å or 6.1 ± 0.4 nm and 75.7 ± 3.2 Å or 7.6 ± 0.3 nm, respectively, and fall within the mesopore region ($2 \text{ nm} < \text{pore diameter} < 50 \text{ nm}$).⁵²

Imprinted microspheres exhibited a much smaller surface area than the non-imprinted microspheres. The sharp drop in surface area was attributed to the presence of hysteresis loop in the adsorption–desorption isotherms of imprinted microspheres (Fig. S5, ESI[†]). Hysteresis effects similar to type III were observed (Fig. S5, ESI[†]). Second, the imprinting effect of

Table 1 Surface area and pore volumes of microspheres (non-imprinted and imprinted)

Adsorbents (microspheres)	Surface area ($\text{m}^2 \text{g}^{-1}$)	Pore size (\AA)
NIPs	222.5 ± 52.9	27.1 ± 5.4
PYMMIPs	40.1 ± 10.0	51.6 ± 7.9
QUNMIPs	76.3 ± 15.1	60.9 ± 4.1
CARMIPs	50.2 ± 17.1	75.7 ± 3.2

NIPs, non-imprinted microspheres; QUNMIPs, quinoline-imprinted microspheres; PYMMIPs, pyrimidine-imprinted microspheres; CARMIPs, carbazole-imprinted microspheres.

templates may have influenced the observed pore diameter and surface area of imprinted microspheres.^{49,50,53,54} Third, the thermodynamic properties of template solvents in the presence of porogen and cross-linker (EGDMA) have been reported to influence the surface area of imprinted microspheres.^{55,56}

3.5 Isothermal titration calorimetry (ITC) studies

The ITC interaction titrations between 2-(1*H*-imidazol-2-yl)-4-phenol and quinoline, pyrimidine and carbazole are presented in Fig. 4. The amount of heat released with the progress in the interaction between nitrogen containing compounds and 2-(1*H*-imidazol-2-yl)-4-phenol with time is presented in Fig. 4.

From the obtained thermodynamic parameters, negative free energies were observed for all interactions (quinoline/2-(1*H*-imidazol-2-yl)-4-phenol, pyrimidine/2-(1*H*-imidazol-2-yl)-4-phenol

and carbazole/2-(1*H*-imidazol-2-yl)-4-phenol) (Table 2). Quinoline-2-(1*H*-imidazol-2-yl)-4-phenol and pyrimidine-2-(1*H*-imidazol-2-yl)-4-phenol interactions proceeded spontaneously compared to the carbazole-2-(1*H*-imidazol-2-yl)-4-phenol interaction. During the adsorption process, the randomness of the interacting molecules decreases, hence giving rise to negative entropies ($-VE \Delta S_b$). The pyrimidine-2-(1*H*-imidazol-2-yl)-4-phenol interaction presented a lower degree of randomness as compared to quinoline-2-(1*H*-imidazol-2-yl)-4-phenol and carbazole-2-(1*H*-imidazol-2-yl)-4-phenol interactions. The positive value of ΔS obtained for carbazole-2-(1*H*-imidazol-2-yl)-4-phenol suggests increased randomness at the solid/solution interface with some structural changes in the adsorbate and adsorbent.

Based on the obtained enthalpy (ΔH_b) values, quinoline-2-(1*H*-imidazol-2-yl)-4-phenol and pyrimidine-2-(1*H*-imidazol-2-yl)-4-phenol offer better interactions (exothermic in nature) as compared carbazole-2-(1*H*-imidazol-2-yl)-4-phenol (endothermic process) (Table 2). The stoichiometry of interaction (n), binding constant (K), free energy (ΔG_b), enthalpy (ΔH_b) and entropy (ΔS_b) are presented in Table 2.

3.6 Van't Hoff study

The Van't Hoff plot was used to determine the thermodynamic parameters such as enthalpy, entropy and Gibbs free energy of the adsorption process.⁵⁷ Thus, ΔH° can be determined from the slope of the linear Van't Hoff plot of K_{ad} versus $(1/T)$.⁵⁸

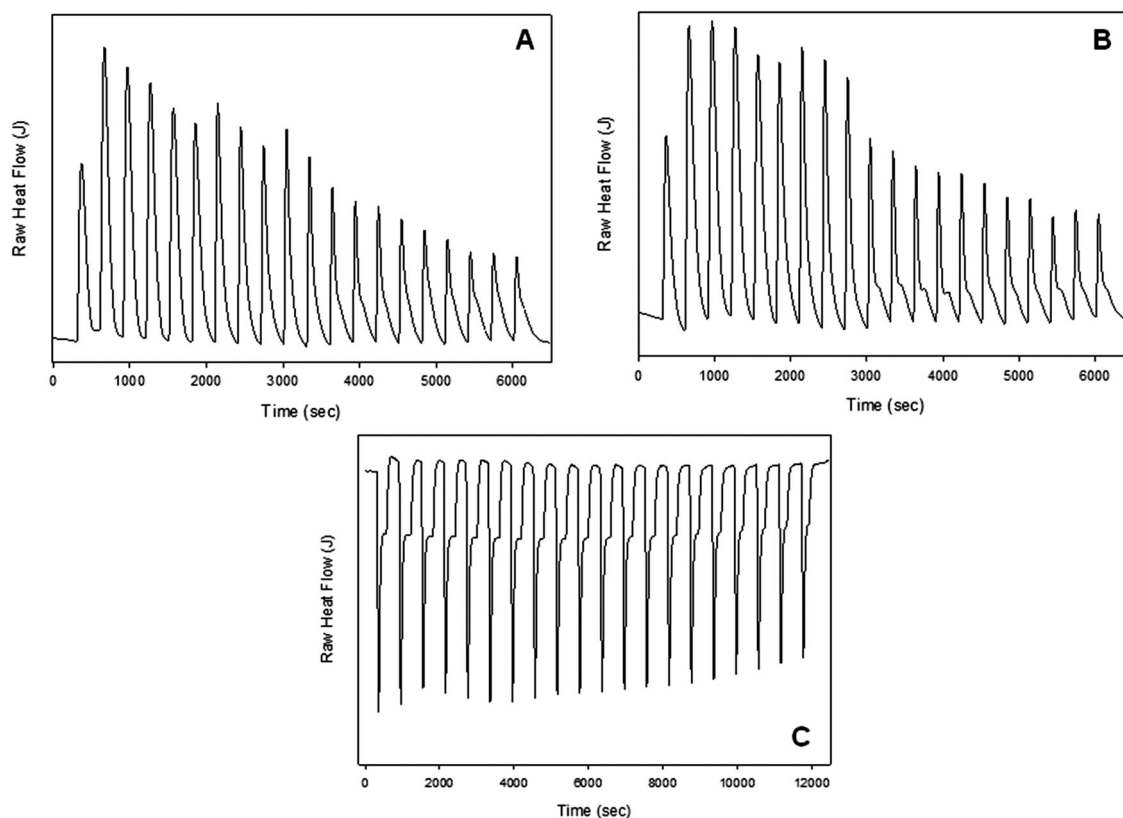


Fig. 4 ITC titration involving 2-(1*H*-imidazol-2-yl)-4-phenol (PIMH) with (A) quinoline, (B) pyrimidine and (C) carbazole. 100 mM (quinoline/pyrimidine/carbazole) was titrated into 20 mM 2-(1*H*-imidazol-2-yl)-4-phenol.

Table 2 Isothermal titration calorimetry (ITC) and Van't Hoff data

Isothermal titration calorimetry (ITC) data						
	Free energy (ΔG_b) (kJ mol ⁻¹)	Stoichiometry of the interaction (n)	Enthalpy (ΔH_b) (kJ mol ⁻¹)	Entropy (ΔS_b) (kJ K ⁻¹)	k	Temperature (K)
PIMH-quinoline	-28.8	0.987 ± 0.046	-18.0 ± 4.8	-10.3	1.1 × 10 ²	298
PIMH-pyrimidine	-30.3	0.914 ± 0.050	-28.1 ± 3.6	-35.3	2.0 × 10 ²	298
PIMH-carbazole	-4.3	1.13 ± 0.01	3.3 ± 0.7	10.9	1.8 × 10 ¹	298
Van't Hoff plot data						
	Free energy (ΔG_b) (kJ mol ⁻¹)	Enthalpy (ΔH_b) (kJ mol ⁻¹) × 10 ⁻²	Entropy (ΔS_b) (kJ K ⁻¹)	Temperature (K)		
PIMH-quinoline	-16.16	-6.74	0.094	298		
PIMH-pyrimidine	-37.44	-48.65	0.124	298		
PIMH-carbazole	-12.29	-7.15	0.041	298		

Fig. S6 (ESI[†]) shows the Van't Hoff's plot for carbazole, quinoline and pyrimidine adsorptions and the calculated thermodynamic values (ΔH° , ΔS° and ΔG_{ad}°) for model organonitrogen compounds are shown in Table 2. Negative ΔG_{ad}° observed for all interactions indicated the feasibility and spontaneity of the adsorption process.

The negative ΔH° values observed for all organonitrogen compounds confirm the exothermic nature of the overall sorption process. The positive value of ΔS° observed for all model organonitrogen compounds suggests increased randomness at the solid/solution interface with some structural changes in the adsorbate and adsorbent and an affinity of molecularly imprinted poly-2-(1*H*-imidazol-2-yl)-4-phenol microspheres towards the various nitrogen containing compounds. The obtained data for carbazole interaction were in contradiction with the results generated from the ITC experiment. Van't Hoff experiments were conducted in two phase systems [solid (microspheres)-liquid (organonitrogen compounds) interaction], while the ITC experiment was conducted in the same phase [liquid (2-(1*H*-imidazol-2-yl)-4-phenol)-liquid (organonitrogen compounds) interaction], hence resulting in the absence of an interface.

3.7 Adsorption studies

3.7.1 Adsorption selectivity studies of imprinted microspheres. Non-imprinted microspheres gave a maximum adsorption of 0.31 mg g⁻¹, 0.35 mg g⁻¹ and 0.24 mg g⁻¹, respectively, for quinoline, carbazole and pyrimidine. Relatively moderate adsorption capacities with no selectivity were observed when NIPs were employed. However, high adsorption capacities were observed when imprinted microspheres were employed to target specific N-compounds: (i) quinoline-imprinted microspheres (QUNMIPs) presented 6.8 ± 0.2 mg g⁻¹ quinoline (Fig. S7, ESI[†]), (ii) pyrimidine-imprinted microspheres (PYMMIPs) presented 6.3 ± 0.3 mg g⁻¹ pyrimidine (Fig. S8, ESI[†]) and (iii) carbazole-imprinted microspheres (CARMIPs) presented 5.8 ± 0.3 mg g⁻¹ carbazole (Fig. S9, ESI[†]). The non-specific binding nature of non-imprinted microspheres gave rise to the non-selective adsorption reported as compared to the imprinted microspheres whose binding sites alongside cavities created *via* imprinting allow for selective adsorption.⁵⁹

Low adsorption capacities were obtained whilst using molecularly imprinted microspheres as compared to adsorption capacities reported in our previous study where molecularly imprinted poly-2-(1*H*-imidazol-2-yl)-4-phenol nanofibers were employed. Molecularly imprinted poly-2-(1*H*-imidazol-2-yl)-4-phenol nanofibers produced adsorption capacities of 11.7 ± 0.9 mg g⁻¹, 11.9 ± 0.8 mg g⁻¹ and 11.3 ± 1.1 mg g⁻¹ for quinoline, pyrimidine and carbazole, respectively, in our recently published article due to the high surface area and available functionalities of the adsorbent.⁵¹ However, the data obtained gave a higher adsorption capacity for quinoline as compared to the reported value for poly-1,1'-binaphthyl-2,2'-diol nanofibers and polybenzimidazole.⁴⁰

Generally, the application of imprinted poly-2-(1*H*-imidazol-2-yl)-4-phenol microspheres as adsorbents for adsorptive denitrogenation of hydrotreated fuel is relatively new and a previous study was carried out using nanofibers which had a higher capacity but poor selectivity.⁶⁰ The crosslinked nature of the microspheres results in specific voids for the imprinted molecules and hence gives better selectivity. In another previous study, where quinoline-*N*-oxide imprinted polybenzimidazole (PBI) nanofibers were employed,⁶¹ the adsorption capacity was lower (4.8 mg g⁻¹) than what is experienced in the adsorption of neat quinoline in this study (6.8 mg g⁻¹). When considering the rate at which equilibrium is reached, our microspheres presented a slower kinetics as compared to the equilibrium time of 90 min reported by Cao and co-workers.³⁵ The observed faster kinetics was probably due to the improved material surface area, particle size and the functional monomer employed (4-vinylpyridine).³⁵ In contrast, our sorbents presented slower kinetics (with equilibrium reached at 300 min) and low materials' surface areas. The observed data may have been influenced by the functional monomer, template and the size of the resulting polymer. Similarly, the high adsorption capacity of 60 mg g⁻¹ reported for indole and carbazole type compounds was attained in 150 min,³⁶ in which case again the adsorbent surface area was above 500 m² g⁻¹. It is obvious that the surface area and the thermodynamic property of the template influence the adsorption kinetics and capacities of MIPs. MOFs and functionalized silica and zeolite are also known to possess large surface areas and pores which enable the adsorption of high concentrations of organonitrogen compounds.^{1,28-33}

Adsorption selectivity increased in the order of quinoline ($\alpha_{i-r} = 136.9$) > pyrimidine ($\alpha_{i-r} = 126.2$) > carbazole ($\alpha_{i-r} = 86.3$). Adsorption selectivity for quinoline was greater than that for pyrimidine and carbazole (Fig. S10, ESI†). This implied that the functional groups and cavities on the surface of the MIP may be quite different, leading to the quite different adsorption selectivity. It also indicated that the surface of imprinted microspheres is likely to have multiple adsorption sites (surface heterogeneity), which contribute to adsorbent-adsorbate interaction. A reduction of $<10 \text{ mg L}^{-1}$ observed for dibenzothiophene and naphthalene (having a similar structural orientation as carbazole and quinoline) was attributed to the imprinting properties of the polymer microspheres. The reduction in dibenzothiophene and naphthalene concentrations could have resulted from π - π stacking between adsorbent and adsorbates (dibenzothiophene and naphthalene).

3.7.2 Imprinting factor (k). The imprinting constant (k) is defined as the ratio of the adsorption capacity of imprinted microspheres (Q_{MIP}) to the adsorption capacity of non-imprinted microspheres (Q_{NIP}). The higher the value of k , the better is the imprinting effect.

$$k = \frac{Q_{\text{MIP}}(\text{Adsorption capacity of the imprinted microspheres})}{Q_{\text{NIP}}(\text{Adsorption capacity of the non-imprinted microspheres})}$$

where k is the imprinting factor, $Q_{\text{NIP}} (\text{mg g}^{-1})$ is the adsorption capacity of non-imprinted microspheres and $Q_{\text{MIP}} (\text{mg g}^{-1})$ is the adsorption capacity of imprinted microspheres.

The imprinting factor (k) value for quinoline-imprinted microspheres is 21.9, for pyrimidine-imprinted microspheres 26.3, and for carbazole-imprinted microspheres 16.6 (Table S1, ESI†).

3.7.3 Adsorption kinetics and isotherm. Adsorption kinetic studies using imprinted microspheres showed that nitrogen molecule adsorption was initially fast due to the availability of surface adsorption and thereafter the adsorption rate slowed down as surface saturation was reached, thus, limiting further nitrogen molecule penetration (Fig. S11, ESI†). The adsorption equilibrium was reached after 5 h. An approximate adsorption rate per hour of 1.32 mg g^{-1} , 1.26 mg g^{-1} , and 1.16 mg g^{-1} was observed for quinoline, pyrimidine and carbazole, respectively.

The pseudo-first-order and pseudo-second-order parameters (coefficients) are presented in Table 3. Based on the obtained correlation coefficients (R^2), carbazole, quinoline and pyrimidine fitted the pseudo-first-order model. The pseudo-first-order model is presented in Fig. 5.

The adsorption behaviour of nitrogen compounds on imprinted nanofibers fitted the Freundlich isotherm (better correlation coefficient R^2 , Fig. 6 and Table 4)⁵⁸ (Fig. S12, ESI†). The Freundlich isotherm indicated multilayer adsorption on the adsorbent surface, implying nitrogen compound-nitrogen compound interactions on the adsorbent.

3.8 Adsorbent reusability studies

Reusability studies on the imprinted microspheres were carried out using the solid phase extraction (SPE) technique.^{59,62} The rebinding adsorption capacities of imprinted microspheres decreased significantly for all nitrogen compounds as we moved from the 1st adsorption cycle to the 3rd cycle for

Table 3 Kinetic data of pseudo-first-order and pseudo-second-order

	Pseudo-first-order kinetics		Pseudo-second-order kinetics	
	$k (\text{h}^{-1})$	R^2	$k_2 (\text{g mg}^{-1} \text{h}^{-1})$	R^2
Quinoline	0.448	0.9992	0.089	0.9078
Carbazole	0.496	0.9724	0.033	0.8634
Pyrimidine	0.547	0.9864	0.005	0.1865

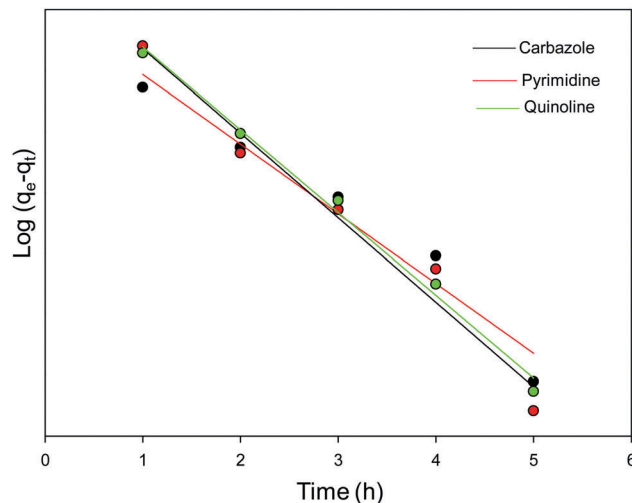


Fig. 5 Pseudo-first-order plot of the nitrogen compounds: pyrimidine, carbazole and quinoline.

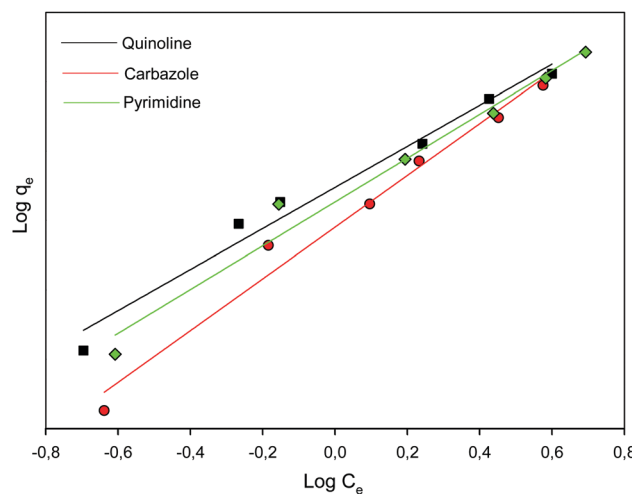


Fig. 6 Freundlich plot for carbazole, quinoline and pyrimidine.

carbazole (Fig. S13, ESI†), quinoline (Fig. S14, ESI†) and pyrimidine (Fig. S15, ESI†). This reduction in adsorption capacities upon employing the microspheres for several cycles indicated that the imprinting integrity may have been compromised.⁵⁸ Table 5 presents the various concentrations of nitrogen containing compounds taken up after each cycle.

3.9 Adsorption of nitrogen compounds in diesel fuel

Prior to denitrogenation, some alkylated organonitrogen compounds were identified in the hydrotreated diesel by employing

Table 4 Parameters of the Langmuir adsorption model and the Freundlich adsorption model

	Langmuir parameters		Freundlich parameters	
	Q_m	R^2	n	R^2
Quinoline	65.79	0.0670	1.06	0.9845
Carbazole	12.56	0.7460	1.02	0.9942
Pyrimidine	0.665	0.8610	1.19	0.9831

Table 5 Various amounts of nitrogen containing compounds absorbed after each adsorption cycle

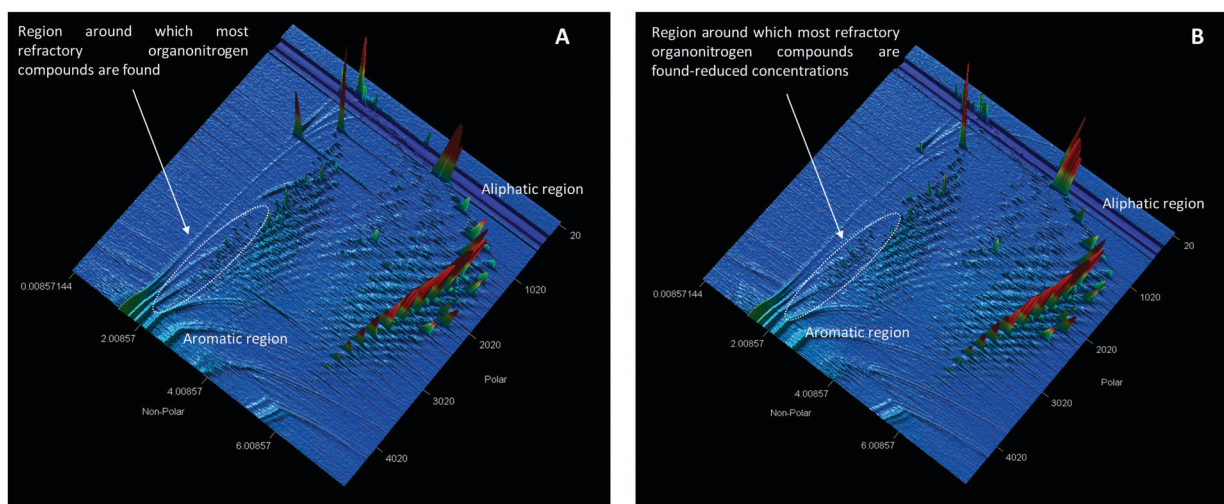
	First adsorption cycle (mg L ⁻¹)	Second adsorption cycle (mg L ⁻¹)	Third adsorption cycle (mg L ⁻¹)
Carbazole	104.5 ± 4.1	93.6 ± 5.6	84.9 ± 3.2
Quinoline	99.6 ± 6.0	87.2 ± 4.2	78.4 ± 3.1
Pyrimidine	98.8 ± 4.2	89.2 ± 4.1	81.7 ± 3.6

NB: initial concentration = 120 mg L⁻¹.

LECO Pegasus GC × GC-HRT (Fig. 7). A reduction in the concentration of alkylated organonitrogen compounds in the hydrotreated fuel was observed after adsorption (Fig. 7). MS data revealed that the peak area of some identified alkylated organonitrogen compounds reduced after adsorption (Table 6). Imprinted adsorbents show promise owing to their ideal physical and chemical characteristics, thus enabling the adsorption of refractory organonitrogen compounds. However, some

complexities were observed as the adsorbent also wiped out some non-imprinted compounds, such as cumidine, 1-phenyl-1-propanamine and 4-pentyloxyaniline. This was attributed to the ability of the adsorbent to easily interact with these compounds *via* hydrogen bonding. Imprinted microspheres were unable to eliminate 3-(*N,N*-dimethylamino)-9-methylcarbazole completely due to the highly alkylated nature of the compound, which inhibited its interactions with the active sites of the adsorbent. 9*H*-Carbazol-3-amine, 9-ethyl- (Table 6), on the other hand, was eliminated as it could easily interact with the polymer microspheres *via* hydrogen bond formation and through pi-pi stacking (a weak interaction). The chemical nature of these unwanted N-compounds in fuel influences the adsorption properties of MIPs in targeting these compounds (Fig. 7).

To confirm the selective ability of imprinted polymers further, another test was performed. A mixture composed of pyrimidine, quinoline and carbazole was prepared firstly and transferred to real diesel (Fig. S16, ESI[†]). Then 150 mg of MIP mixture (CARMIPs, PYMMIPs, and PYMMIPs) was added to the mixture. When the absorption equilibrium was achieved (5 h), the adsorbed amounts of pyrimidine, quinoline and carbazole were determined using GC (Fig. S16, ESI[†]). A reduction in the concentrations (peak areas) of pyrimidine, quinoline and carbazole was observed in the hydrotreated fuel after adsorption (Fig. S16, ESI[†]). The plot in Fig. 8 shows the percentage reduction of target nitrogen-containing compounds in diesel oil.

**Fig. 7** GC × GC-high-resolution TOF-MS surface plot showing (A) surface contour plot of hydrotreated diesel (XIC) and (B) surface contour plot (XIC) after adsorption of hydrotreated diesel fuel.**Table 6** Some alkylated organonitrogen compounds found before and after the adsorption of hydrotreated fuel

Name	Formula	R.T. (s)	Base mass	Area (before adsorption)	Area (after adsorption)
Cumidine	C ₉ H ₁₃ N	1723.39, 3.35143	1 200 932	4676	ND
1-Phenyl-1-propanamine	C ₉ H ₁₃ N	1915.33, 3.32572	1 060 777	95 933	ND
4-Pentyloxyaniline	C ₁₁ H ₁₇ NO	2930.96, 5.05715	1 091 012	47 285	ND
1-Methyl-2,5-dipropyldecahydroquinoline	C ₁₆ H ₃₁ N	4002.58, 2.34857	1 941 088	7818	ND
3-(<i>N,N</i> -Dimethylamino)-9-methylcarbazole	C ₁₅ H ₁₆ N ₂	4002.58, 2.48982	2 241 195	42 756	11 525
9 <i>H</i> -Carbazol-3-amine, 9-ethyl	C ₁₄ H ₁₄ N ₂	3954.6, 2.50286	2 101 401	30 379	ND
2-Butyl-1-pyrroline	C ₈ H ₁₅ N	3478.83, 2.91429	830 855	25 596	ND

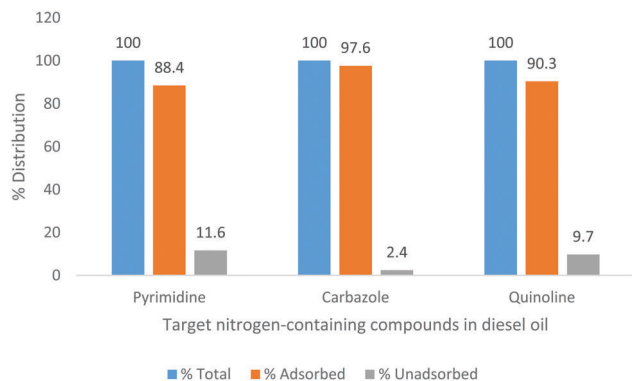


Fig. 8 Percentage distribution of target nitrogen-containing compounds in diesel oil.

A total of 88.4%, 97.6% and 90.3% was selectively adsorbed for pyrimidine, carbazole and quinoline, respectively (Fig. 8). The corresponding adsorption amounts for pyrimidine, carbazole and quinoline were 10.56 mg g^{-1} , 11.71 mg g^{-1} and 10.84 mg g^{-1} , respectively, in the real diesel oil solution (200 mg L^{-1}).

4. Conclusions

Molecularly imprinted 2-(1*H*-imidazol-2-yl)-4-phenol showed enhanced adsorption capacities and selectivity for individual nitrogen compounds due to their specific binding nature. A better regression R^2 presented by the Freundlich isotherm confirmed multilayer adsorption attributed to the interactions between imprinted microspheres and nitrogen compounds, and possibly between nitrogen molecules. The adsorbent materials which exhibit hydrophobic interactions (van der Waals or dispersion forces) and hydrophilic interactions (hydrogen bonding, pi-pi interactions, dipole-dipole interactions) based on SPE presented a more efficient and quantitative extraction of N-compounds in fuels. Isothermal titration calorimetry (ITC) revealed that quinoline-PIMH and pyrimidine-PIMH interactions are exothermic in nature, while the carbazole-PIMH interaction is endothermic in nature. A significant reduction in the quantity of nitrogen compounds in hydrotreated fuel was observed (peak area reduction) when imprinted 2-(1*H*-imidazol-2-yl)-4-phenol microspheres were employed; however, the complex nature of N-compounds in fuel influences the imprinting properties of MIPs for targeting these unwanted compounds. The spectroscopic analysis of all synthesised microspheres allows for a clear identification of the possibility of forming a chromophore when pyrimidine is employed as a template.

Conflicts of interest

There are no conflicts to declare.

Acknowledgements

We highly acknowledge financial support to the project in the form of research grant from the South African National Research Foundation and Sasol (Pty) Ltd.

References

- 1 J. Ahmed, N. A. Khan, Z. Hasan and J. H. Jhung, *J. Hazard. Mater.*, 2013, **250–251**, 37.
- 2 V. C. Srivastava, *RSC Adv.*, 2012, **2**, 759.
- 3 Q. Shi, D. Hou, K. H. Chung, C. Xu, S. Zhao and Y. Zhang, *Energy Fuels*, 2010, **24**, 2545.
- 4 Q. Wei, S. Wen, X. Tao, T. Zhang, Y. Zhou, K. Chung and C. Xu, *Fuel Process. Technol.*, 2015, **129**, 76.
- 5 G. C. Laredo, P. M. Vega-Merino, F. Trejo-Zárraga and J. Castillo, *Fuel Process. Technol.*, 2013, **106**, 21.
- 6 M. Z. M. Salleh, M. K. Hadj-Kalic, H. F. Hizaddin and M. A. Hashima, *Sep. Sci. Technol.*, 2018, **61**, 196.
- 7 G. C. Laredo, N. V. Likhanova, I. V. Lijanova, B. Rodriguez-Heredia, J. J. Castillo and P. Perez-Romo, *Fuel Process. Technol.*, 2015, **130**, 38.
- 8 J. W. Bauserman, K. M. Nguyen and G. W. Mushrush, *Pet. Sci. Technol.*, 2004, **22**, 1491.
- 9 L. Xe., F.-R. Alain, P.-R. Stephane, X. X. Wang, X. Fu, J. Estager, M. Vrinat and M. Lemaire, *Ind. Eng. Chem. Res.*, 2008, **47**, 8801.
- 10 C. A. Hughey and S. A. Glassow, *Fuel*, 2007, **86**(56), 758.
- 11 H. Zhang, G. Li, Y. Jia and H. Liu, *J. Chem. Eng. Data*, 2010, **55**, 173.
- 12 I. Ahmed and S. H. Jhung, *J. Hazard. Mater.*, 2016, **301**, 259.
- 13 B. Pawelec, R. M. Navarro, J. M. Campos-Martin and J. L. G. Fierro, *Catal. Sci. Technol.*, 2011, **1**, 23.
- 14 J. W. Bauserman, G. W. Mushrush and D. R. Hardy, *Ind. Eng. Chem. Res.*, 2008, **47**, 2867.
- 15 P. W. Seo, I. Ahmed and S. H. Jhung, *Chem. Eng. J.*, 2016, **299**, 236.
- 16 A. Jayaraman, F. H. Yang and R. T. Yang, *Energy Fuels*, 2006, **20**, 909.
- 17 V. C. Srivastava, *RSC Adv.*, 2012, **2**, 759.
- 18 X. Fan, G.-F. Liu, Z.-M. Zong, X.-Y. Zhao, J. P. Cao, B.-M. Li, W. Zhao and X.-Y. Wei, *Fuel Process. Technol.*, 2013, **106**, 661.
- 19 M. Almari, X. Ma and C. Song, *Ind. Eng. Chem. Res.*, 2009, **48**, 951.
- 20 J. H. Maldonado and R. T. Yang, *Angew. Chem., Int. Ed.*, 2004, **43**, 1004.
- 21 G. C. Laredo, S. Leyva, R. Alvarez, M. T. Mares, J. Castillo and J. L. Cano, *Fuel*, 2002, **81**, 1341.
- 22 Y. Sano, K.-H. Choi, Y. Korai and I. Mochida, *Energy Fuels*, 2004, **18**, 644.
- 23 J. When, X. Han, H. Lin, Y. Zheng and W. Chu, *Chem. Eng. J.*, 2010, **164**, 29.
- 24 A. L. Nuzhdin, K. A. Kovalenko, D. N. Dybtsev and G. A. Bukhtiyarova, *Mendeleev Commun.*, 2010, **20**, 57.
- 25 D. Liu, J. Gui and Z. Sun, *J. Mol. Catal. A: Chem.*, 2008, **291**, 17.
- 26 L. L. Xie, A. Farre-Reguillon, X.-X. Wang, X. Fu and M. Lemaire, *J. Chem. Eng. Data*, 2010, **55**, 4849.
- 27 I. Ahmed, J. W. Jun, B. K. Jung and S. H. Jhung, *Chem. Eng. J.*, 2014, **255**, 623.
- 28 G. Férey, *Chem. Soc. Rev.*, 2008, **37**, 191.
- 29 S. Kitagawa, R. Kitaura and S. I. Noro, *Angew. Chem., Int. Ed.*, 2004, **43**, 2334.

- 30 O. M. Yaghi, M. O'Keeffe, N. W. Ockwig, H. K. Chae, M. Eddaoudi and J. Kim, *Nature*, 2003, **423**, 705.
- 31 N. A. Khan, Z. Hasan and S. H. Jhung, *J. Hazard. Mater.*, 2012, **244–245**, 444.
- 32 S. H. Jhung, N. A. Khan and Z. Hasan, *CrystEngComm*, 2012, **14**, 7099.
- 33 J. Kim, X. Ma, A. Zhou and C. Song, *Catal. Today*, 2006, **111**, 74.
- 34 A. S. Ogunlaja, C. du Sautoy, N. Torto and Z. R. Tshentu, *Talanta*, 2014, **126**, 61.
- 35 Y. Cao, L. Liu, W. Xu, X. Wu and W. Huang, *J. Appl. Polym. Sci.*, 2014, **131**, 40473.
- 36 W. Yang, L. Liu, Z. Zhou, C. Qiu, P. Ma, H. Liu and W. Xu, *New J. Chem.*, 2013, **37**, 2758.
- 37 B. Sellergren, R. N. Karmalkar and K. J. Shea, *J. Org. Chem.*, 2000, **65**, 4009.
- 38 G. Krainer, J. Broecker, C. Vargas, J. Fanghänel and S. Keller, *Anal. Chem.*, 2012, **84**, 10715.
- 39 O. Callies and A. Hernández Daranas, *Nat. Prod. Rep.*, 2016, **33**, 881.
- 40 A. S. Ogunlaja, E. Hosten, R. Betz and Z. R. Tshentu, *RSC Adv.*, 2016, **6**, 39024.
- 41 C. Schönbeck, R. Holm and P. Westh, *Anal. Chem.*, 2012, **84**, 2305.
- 42 K. Rajarathnam and J. Rösigen, *Biochim. Biophys. Acta, Biomembr.*, 2014, **1838**, 69.
- 43 L. N. Wafer, W. W. Streicher, S. A. McCullum and G. I. Makhatadze, *Biochemistry*, 2012, **51**, 7189.
- 44 O. Khakshoor, S. E. Wheeler, K. N. Houk and E. T. Kool, *J. Am. Chem. Soc.*, 2012, **134**, 3154.
- 45 X. Wang, E. Matei, A. M. Gronenborn, O. Ramström and M. Yan, *Anal. Chem.*, 2012, **84**, 4248.
- 46 S. Keller, H. Heerklotz and A. Blume, *J. Am. Chem. Soc.*, 2006, **128**, 1279.
- 47 J. M. D. Trani, S. De Cesco, R. O'Leary, J. Plescia, C. J. do Nascimento, N. Moitessier and A. K. Mittermaier, *Nat. Commun.*, 2018, **9**, 893.
- 48 W. F. Su, in *Principles of Polymer Design and Synthesis*, Lecture Notes in Chemistry, Springer, Berlin, Heidelberg, 2013, vol. 82, p. 89.
- 49 L. A. Tom, N. A. Schneck and C. Walter, *J. Chromatogr. B: Anal. Technol. Biomed. Life Sci.*, 2012, **909**, 61.
- 50 K. Golker and I. A. Nicholls, *Eur. Polym. J.*, 2016, **75**, 423.
- 51 Y. J. Yang, J. Y. Li, Y. R. Liu., J. Y. Zhang., B. Li and X. P. Cai, *Anal. Bioanal. Chem.*, 2011, **400**, 3665.
- 52 S. A. Nabavi, G. T. Vladislavljevic, E. M. Eguagie, B. Li, S. Georgiadou and V. Manovic, *Chem. Eng. J.*, 2016, **306**, 214.
- 53 P. Li, C. Mu, T. Wang, F. Lei, H. Li, Q. Huang and J. Zhou, *S. Afr. J. Chem.*, 2014, **67**, 67.
- 54 H. Y. Yuan, X. H. Ma and Z. L. Xu, *Sci. China: Chem.*, 2011, **54**, 257.
- 55 M. J. Whitcombe, N. Kirsch and I. A. Nicholls, *J. Mol. Recognit.*, 2014, **27**(6), 297.
- 56 P. A. G. Cormack and A. Z. Elorza, *J. Chromatogr. B: Anal. Technol. Biomed. Life Sci.*, 2004, **804**, 173.
- 57 F. Gritti and G. Guiochon, *Anal. Chem.*, 2006, **78**, 4642.
- 58 A. S. Ogunlaja, C. J. Mathew, N. Torto and Z. R. Tshentu, *React. Funct. Polym.*, 2014, **81**, 61.
- 59 X. Liu, Y. P. Guan, Q. Wang, X. F. Ren and M. Z. Yang, *J. Appl. Polym. Sci.*, 2012, **126**, 1956.
- 60 M. S. Abdul-quadir, E. E. Ferg, Z. R. Tshentu and A. S. Ogunlaja, *RSC Adv.*, 2018, **8**, 8039.
- 61 A. S. Ogunlaja, M. S. Abdul-quadir, P. E. Kleyi, E. E. Ferg, P. Watts and Z. R. Tshentu, *Arabian J. Chem.*, 2017, DOI: 10.1016/j.arabjc.2017.05.010.
- 62 A. Zwir-Ferenc and M. Bizuik, *Pol. J. Environ. Stud.*, 2006, **15**(5), 677.